Numerical Analysis of Spray Phenomena in Fuel Injection Engines

T.Wakisaka, Y.Shimamoto, Y.Isshiki*, T.Noda**, A.Matsui and S.Akamatsu

Department of Mechanical Engineering
Kyoto University
Yoshida, Sakyo-ku, Kyoto 606-01
Japan
* *Setsunan University*
** *Nissan Motor Corporation*

ABSTRACT

As a model for fuel sprays impinging on a wall with liquid film formation, a new model is proposed in this study. The model treats the liquid film as a group of "Liquid Film Elements". This model is incorporated into the authors' GTT code, which employs the Discrete Droplet Model (DDM) in the KIVA code along with the drop breakup model by Reitz et al. The present spray model has been tested for sprays injected in quiescent and swirling gases. By comparing the calculated results with the experimental data, the validity of the model has been confirmed, though some improvements of the drop breakup model are necessary. With respect to sprays impinging on a flat wall, it has been found that the present spray model gives good predictions for the behavior of droplets and liquid film and for the adherent fuel mass ratio. Using the present spray model, the behavior of sprays with liquid film formation in a port-injection gasoline engine has been numerically simulated, and the process of mixture formation during intake stroke has been analyzed.

INTRODUCTION

In order to numerically analyze the spray phenomena in liquid fuel injection engines, various spray models such as the Discrete Droplet Model[1] have been proposed. At present, however, no model can correctly predict the whole phenomena of sprays including the behavior of sprays impinging on walls and the formation of liquid film. The authors have developed a model for sprays impinging on a wall[2], but have not taken the liquid film into consideration. In this study, a new submodel to treat the behavior of the liquid film formed by sprays impinging on a wall is proposed. The submodel is combined with the previous spray model to construct a new model for sprays impinging on a wall with liquid film formation. This model is incorporated into the authors' GTT (Generalized Tank and Tube) code[3], which employs the Discrete Droplet Model in the KIVA code[1] along with the drop breakup model by Reitz et al.[4]. In this breakup model, drop breakup is treated in the bag and stripping breakup modes. As the submodel of droplet coalescence, the model in the KIVA code is used in this study. Fundamental examination of the present spray model in the GTT code is carried out with respect to the free sprays injected in high-pressure, room- or high-temperature quiescent gas and the sprays injected in high-pressure, room-temperature swirling gas, and also with respect to the sprays impinging on a flat wall in high-pressure, room-temperature quiescent gas. Furthermore, using the present spray model, the spray behavior and the liquid film formation in a port-injection gasoline engine have been numerically analyzed.

METHOD OF NUMERICAL ANALYSIS

The GTT code calculates gas flows in engines by means of fully-implicit algorithm based on a finite volume method with generalized curvilinear coordinates, using the $k-\varepsilon$ two-equation model as a turbulence model. As the differencing scheme of convection terms, the QUICK scheme is used for Navier-Stokes equations, and the Hybrid scheme is used for the conservation equations of enthalpy, turbulence energy k and its dissipation rate ε. Pressure-velocity coupling is accomplished by means of the SIMPLEC algorithm. Concerning the interaction between the gas and fuel droplets, the vaporized mass, momentum and enthalpy lost by the droplets are given to the source terms in their respective conservation equations as to the gas phase. The time increment Δt for calculating the velocity field is set at 0.05 - 0.15 ms, and the spray behavior is calculated explicitly in subcycles with a smaller time increment Δt_s ($=1/10$ - $1/25\ \Delta t$). The concentration field of fuel vapor is calculated explicitly in subcycles using the CIP method[5], whose false diffusion is very small. All the calculations with respect to spray phenomena in this study are carried out using engineering work stations.

SIMULATION OF FREE SPRAYS

The behavior of free sprays under the conditions of the experiment by Hiroyasu et al.[6] is numerically simulated to compare the calculated results with their experimental data. In their experiment, diesel fuel oil is injected from a single-hole nozzle into a vessel filled with high-pressure, quiescent nitrogen gas at room temperature. The injection pressure is 9.9 MPa. The details of test conditions are shown in Table 1. The computational grid used is shown in Fig.1. The droplet injection velocity is determined on the basis of the pressure difference,

fuel density and the flow coefficient of the injector nozzle according to Ref.(7). The injection cone angle of spray is determined using the empirical equation by Reitz et al.[4]. The initial droplet radius is equated to the nozzle diameter (0.3 mm), and the injection fuel rate is set at constant. The number of injected droplet parcels (representative particles of droplets) is 2000. As an example, the shape of calculated sprays for Case 4 is shown in Fig.2. The calculated results of the spray tip penetration are shown in Fig.3 along with the experimental data[6]. The position of the spray tip is defined as the position where 10 % of the total injected fuel mass has passed. It is found that the calculated results agree well with the experimental data at various ambient gas pressures.

Figure 4 shows the comparison of the calculated and measured[6] Sauter mean radii $\bar{r}_{32}$. The calculated values of $\bar{r}_{32}$ at the various ambient gas pressures except for 0.1 MPa agree considerably well with the measured values. At 0.1 MPa, the calculated $\bar{r}_{32}$ is much larger than the measured value. This means that the drop breakup model used in this study cannot predict the breakup process in low-pressure ambient gas. Therefore, the breakup model has to be improved for predicting the droplet radius distribution under such a condition.

Figure 5 shows the calculated and measured[6] spray cone angles. Here, the cone angle of spray is determined from the spray boundary at the middle section between the nozzle outlet and the spray tip. Although the cone angles of calculated sprays at high ambient gas pressures are larger than the measured ones, a tendency for the spray cone angle to increase with an increase in the ambient gas pressure is predicted.

In order to examine the spray tip penetration in high-temperature ambient gas, the fuel spray injected into the high-temperature (900 K), high-pressure (3.6 MPa) quiescent gas is calculated (Case T1). The spray injected into the room-temperature (300 K), high-pressure (1.5 MPa) quiescent gas is also calculated (Case T0). The ambient gas is nitrogen and the injected fuel is tridecane. The diameter of injector nozzle is 0.16 mm. The pressure difference for injection is 30 MPa and the injection velocity is 185 m/s for both cases. In Fig.6, the calculated results of spray tip penetration (liquid phase) are compared with the measured data[8],[9]. It is found that the spray tip penetration is well predicted in both room- and high-temperature ambient gases by the present spray model.

SIMULATION OF SPRAYS IN SWIRL

The sprays injected into a vessel with swirl are numerically simulated under the conditions of the experiment by Hiroyasu et al.[10]. They used a thin cylindrical vessel having a swirler (rotating vane) at the bottom of the vessel. In this study, the radius r_c and thickness l_c of the computational domain are set at 60 mm and 20 mm, respectively, and the liquid fuel (tridecane) is injected radially from a nozzle (diameter=0.21 mm) located at the center of the vessel. As shown in Fig.7, the computational grid lines are concentrated in the vicinity of the spray axis. High-pressure (1.1 MPa), room-temperature (293 K) air is used to fill in this vessel. In the simulation, the swirl having the measured velocity profile is given in the vessel

Table 1 Test conditions for free sprays

Case	Ambient gas pressure P_g MPa	Ambient gas density (N_2) ρ_g kg/m^3	Injection velocity V_0 m/s	Injection cone angle θ_0 deg.
1	0.1	1.13	107	2.9
2	1.1	12.4	101	9.7
3	2.1	23.7	95	13.4
4	3.0	33.9	90	16.0
5	5.0	56.5	86	20.6

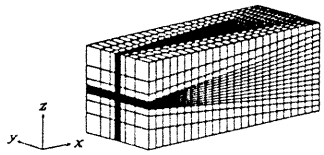

Fig. 1 Computational grid for free sprays (24 × 16 × 16)

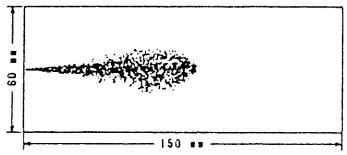

Fig. 2 Spray shape at $t = 4.2$ ms for Case 4 (projections of all droplet parcels)

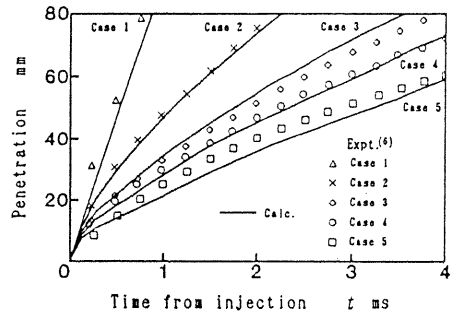

Fig. 3 Spray tip penetration for Case 1 – Case 5

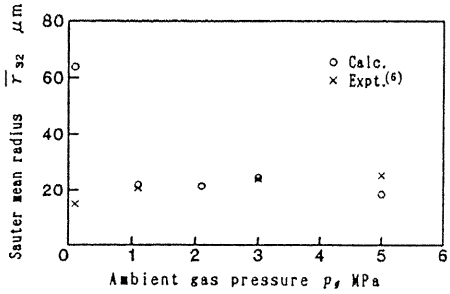

Fig. 4 Effect of ambient gas pressure on Sauter mean radius

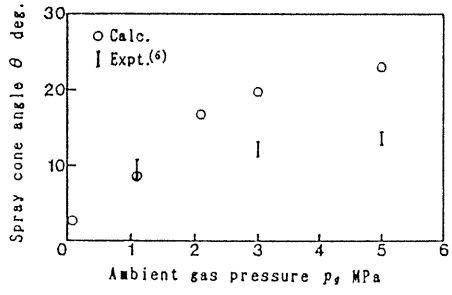

Fig. 5 Effect of ambient gas pressure on spray cone angle

as an initial velocity field. According to the measurement, the rotation speed of the swirl was nearly the same as that of the swirler, which was changed from 0 to 10000 rpm. The initial values for the $k-\varepsilon$ turbulence model, k_i and ε_i, are given as follows:

$$k_i = C(\pi n_s r_c/60)^2 ,$$

$$\varepsilon_i = C_\mu{}^{0.75} k_i{}^{1.5}/(0.07 l_c) ,$$

where n_s = rotation speed of the swirler (rpm), $C = 0.2$ and $C_\mu = 0.09$.

Calculation is carried out under the conditions of $n_s = 0$, 3000 and 7500 rpm, which are designated Case S0, Case S1 and Case S2, respectively. As an example, the calculated result of droplet size and distribution at $t = 2.1$ ms (t = time from injection) for Case S2 is shown in Fig.8. It is found that the droplets are carried in the direction of swirl rotation (counterclockwise) and smaller droplets are distributed in the downstream region of the swirl. The calculated and measured[10] results of the spray tip penetration for Cases S0, S1 and S2 are shown in Fig.9. Here, the spray tip penetration is determined in the same way as the measurement. Namely, the penetration is defined as the radius of a circle, which has a center located at the nozzle outlet and touches the farthest boundary of curved spray. It is found that the calculated results of the spray tip penetration agree reasonably well with the measured results for every cases.

Figure 10 shows the temporal variation in the calculated spray shapes (projections of all droplet parcels) for Case S1 and Case S2. Sprays are curved by the swirl and are dispersed widely near the spray tip. The dispersion becomes wider with an increase in the rotation speed of swirl. In Fig.10, the outlines of measured sprays[10] are also plotted on the plots of the calculated sprays to compare their shapes. It is found that for Case S1, namely at low swirl rotation speed, the calculated spray shape resembles the measured one. However, for Case S2, namely at high swirl rotation speed, the calculated spray shape differs from the measured one. The dispersion of the calculated spray at the part near the tip is too large, while the dispersion at the part near the nozzle is too small. It is found from Fig.8 that the droplet diameter near the nozzle is large because drop breakup does not occur frequently in this region in the case of the breakup model employed in this study, and therefore the droplets scarcely disperse at the part near the nozzle. Consequently, it is necessary to improve the present drop breakup model for predicting the spray dispersion in intense swirl, namely, in high-speed transverse flow.

SIMULATION OF SPRAYS IMPINGING ON A WALL

Model for Sprays Impinging on a Wall with Liquid Film Formation

In this study, the liquid film formed by sprays impinging on a wall is treated as a group of "Liquid Film Elements". For calculating the behavior of a large number of liquid film elements, "Liquid Film Parcels" based on the concept of droplet parcels in the Discrete Droplet Model are introduced. Namely, a liquid film parcel is composed of liquid film elements having the same size and identical properties. When droplets in a droplet parcel impinge on

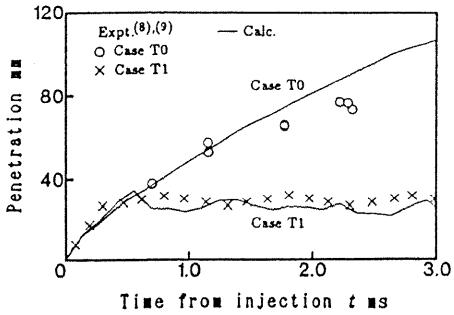

Fig. 6 Spray tip penetration for Case T0 and Case T1

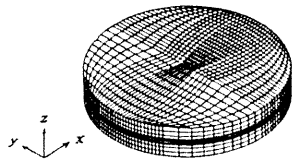

Fig. 7 Computational grid for a thin cylindrical vessel (30 × 30 × 10)

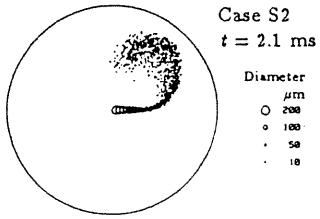

Fig. 8 Droplet size and distribution at $t = 2.1$ ms for Case S2 (projections of all droplet parcels)

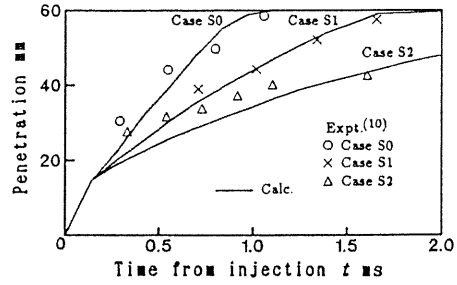

Fig. 9 Spray tip penetration for Cases S0, S1 and S2 (n_s = 0, 3000, 7500 rpm for Cases S0, S1 and S2)

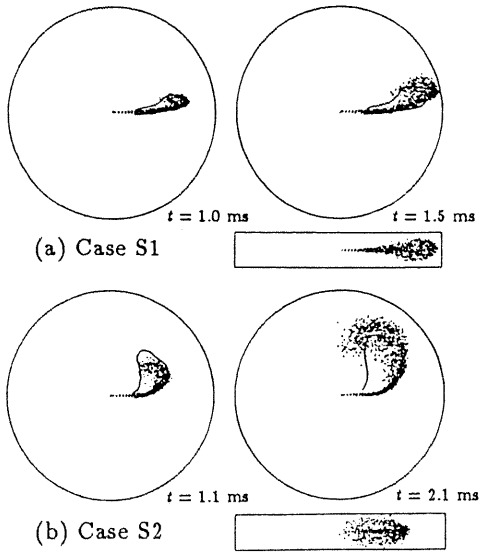

Fig. 10 Temporal variation in spray shapes for Case S1 and Case S2 (solid lines show the measured spray shapes[10].)

a wall and then adhere to the wall without rebounding under certain conditions, the droplets are converted individually into liquid film elements in the liquid film parcel corresponding to the droplet parcel on the assumption that one droplet forms one liquid film element. The group of these liquid film parcels is regarded as the liquid film. The liquid film parcel is the minimum unit for treating the motion of liquid film. It is assumed that these parcels move independently with one another, and their collision, coalescence and breakup are not taken into consideration.

It is assumed that the behavior of a droplet at the moment of impingement on a wall, which is still or moving, is classified into the following three categories according to the incident Weber number of the droplet

$$We = \rho_l (v_d)_n{}^2 r_d / \sigma_l \ ,$$

where ρ_l = droplet density, $(v_d)_n$ = normal component of the droplet velocity relative to the wall, r_d = droplet radius, and σ_l = surface tension. In the following, We_{c_1} and We_{c_2} are critical Weber numbers:

(i) For $We < We_{c_1}$: The droplet rebounds after impingement. The tangential velocity component does not change, but the normal velocity decreases according to the following empirical equation by Jayaratne et al.[11]:

$$\left[(v_d)_{\rm in}{}^2 - (v_d)_{\rm out}{}^2\right] / (v_d)_{\rm in}{}^2 = 0.95 \sin^2 \theta_{\rm in} \ ,$$

where $(v_d)_{\rm in}$ = incident velocity relative to the wall, $(v_d)_{\rm out}$ = reflection velocity relative to the wall, and $\theta_{\rm in}$ = angle between incident direction and wall surface.

(ii) For $We_{c_1} \leqq We \leqq We_{c_2}$: The droplet adheres to the wall at the moment of impingement.

(iii) For $We > We_{c_2}$: As shown in Fig.11, the adhesion probability of a droplet, f, is defined. Droplets impinging on the wall adhere to the wall according to this probability f. Droplets which do not adhere to the wall break up into small droplets of the same radius r_d/n_b, and they rebound in random directions. It is assumed that the magnitude of velocity does not change before and after impingement.

In the above cases (ii) and (iii), it is assumed that adherent droplets become disk-like liquid film elements individually. The initial radius r_f and thickness h_f of the liquid film element are determined using the following empirical equations by Toda[12]:

$$r_f = 1.28 \nu_l{}^{-0.2} r_d{}^{1.2} \ ,$$

$$h_f = 0.82 \nu_l{}^{0.4} r_d{}^{0.6} \ ,$$

(the unit is SI unit: ν_l = kinematic viscosity of the droplet).

The initial velocity of the liquid film element along the wall is given by the Jet Model by Naber[13]. Furthermore, the Reynolds number of the liquid film element

$$Re_f = |\vec{v}_f - \vec{v}_w| h_f / \nu_l$$

($\vec{v}_f$ = velocity of liquid film element, $\vec{v}_w$ = velocity of wall) is examined, and if its value is larger than a critical value Re_c, which is set at 85 in this study, the liquid film element again splashes into the gas in the form of small droplets. This simulates the breakup of the liquid film due to its instability. This process is treated in the same way as the breakup and rebound process in the above case (iii). As in the previous study[2], the following values are given:

$We_{c_1} = 40$ (Ref.(14)), $We_{c_2} = 300$ and $n_b = 2$.

The motion of each liquid film parcel is calculated at each time step in the subcycles by the Lagrangian method on the basis of the equation of motion for each parcel. The surface tension and gravity are ignored. The external forces imposed on a liquid film parcel are treated as follows according to the coverage fraction B_f of liquid film elements over a wall cell (computational grid on a wall)

$$B_f = \textstyle\sum_{\rm p} (\pi r_f{}^2 n_f) / A_{\rm cell} \ ,$$

where $\sum_{\rm p}$ = summation for parcels on a wall cell, n_f = number of liquid film elements in a liquid film parcel, and $A_{\rm cell}$ = area of wall cell:

(a) For $B_f < 1$: It is assumed that the liquid film parcels on the wall cell form disk-like small patches of liquid film separately. The force due to shear stress between the parcel and the wall, $\vec{F}_{r_w}$, is calculated as follows:

$$\vec{F}_{r_w} = \pi r_f{}^2 n_f \mu_l (\vec{v}_w - \vec{v}_f) / (0.5 h_f) \ ,$$

(μ_l = viscosity of liquid film).

The force due to shear stress between the parcel and the gas, $\vec{F}_{r_g}$, is calculated on the basis of the velocity difference between the parcel and the gas by applying the law of the wall. The effect of gas pressure distribution on the parcel is ignored.

(b) For $B_f \geqq 1$: It is assumed that the liquid film parcels fill up the wall cell in a block of liquid film. The liquid film thickness H_f is determined as follows:

$$H_f = \textstyle\sum_{\rm p} (\pi r_f{}^2 h_f n_f) / A_{\rm cell} \ .$$

The force due to shear stress between the parcel and the wall, $\vec{F}_{r_w}$, is calculated as follows:

$$\vec{F}_{r_w} = A_{\rm cell} \mu_l (\vec{v}_w - \vec{v}_{f_m}) / (0.5 H_f) \ ,$$

($\vec{v}_{f_m}$ = mass averaged velocity, relative to the wall, of the liquid film parcels on the wall cell).

The force due to shear stress between the block of liquid film and the gas, $\vec{F}_{r_g}$, is calculated on the basis of the velocity difference between the block and the gas by applying the law of the wall. The effect of gas pressure distribution on the block of liquid film is taken into consideration. These external forces are distributed to each liquid film parcel on the wall cell according to the mass of each parcel. Each liquid film parcel is made to slide along the wall except that the parcel is ejected into the gas when it passes an acute-angled edge of the wall.

The phenomena of heat transfer and evaporation are modeled similarly on the basis of the liquid film elements and parcels.

Validation of the Model

The sprays impinging on a flat wall in high-pressure quiescent gas at room temperature are numerically analyzed under the conditions of the experiments by M. Saito[15] (Case W1) and A. Saito[16] (Case W2). The details of test conditions are shown in Table.2. The computational grid for Case W1 is shown in Fig.12. The fuel used is the JIS #2 light diesel fuel oil. The number of injected droplet parcels is 4000. As an example, simultaneous plotting of the droplet and liquid film parcels at α_w = 30 deg. for Case W1 is shown in Fig.13. Here, α_w is the angle between the spray axis and the wall perpendicular. Figure 14 shows the temporal variation in the distribution of the droplet and liquid film parcels at α_w = 0 deg. for Case W1.

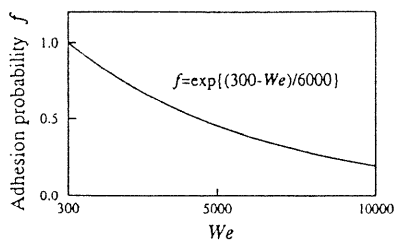

Fig. 11 Adhesion probability of a droplet

Table 2 Test conditions for sprays impinging on a flat wall

		Case W1	Case W2
Ambient gas		Air	N_2
Ambient gas pressure	MPa	1.5	2.1
Injector nozzle diameter	mm	0.20	0.25
Mean injection pressure	MPa	13.8	30.0
Injection velocity	m/s	143	181
Injection cone angle	deg.	10.0	13.4
Injection fuel amount	mm^3	6.63	35.0
Distance to wall	mm	24	25

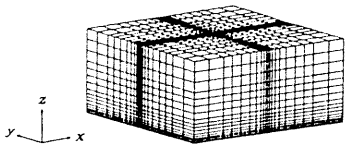

Fig. 12 Computational grid for Case W1 ($\alpha_w = 0$ deg.) ($20 \times 20 \times 16$)

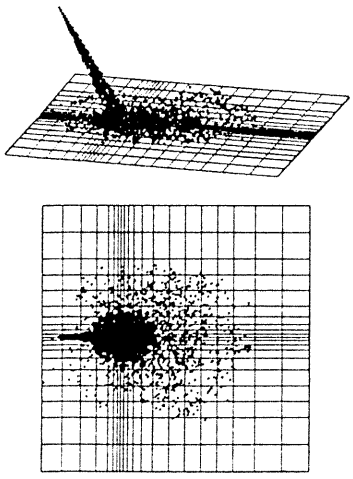

View from bottom

Fig. 13 Simultaneous plotting of the droplet and liquid film parcels at $t = 1.4$ ms for Case W1 ($\alpha_w = 30$ deg.)

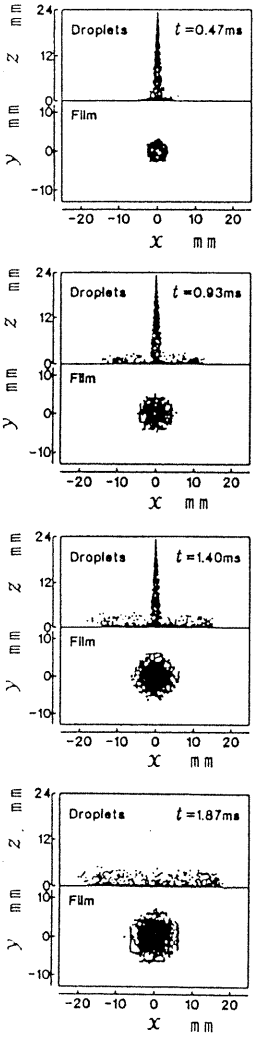

Fig. 14 Temporal variation in the distribution of the droplet and liquid film parcels for Case W1 ($\alpha_w = 0$ deg.)

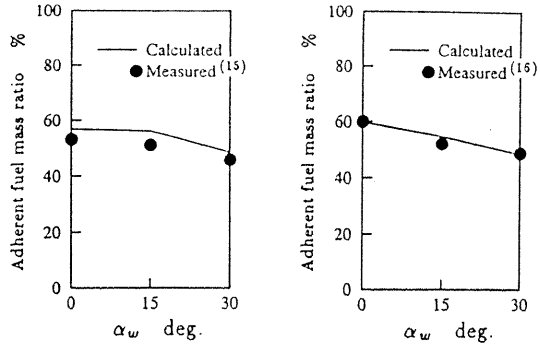

(a) Case W1 (b) Case W2

Fig. 15 Effect of α_w on adherent fuel mass ratio

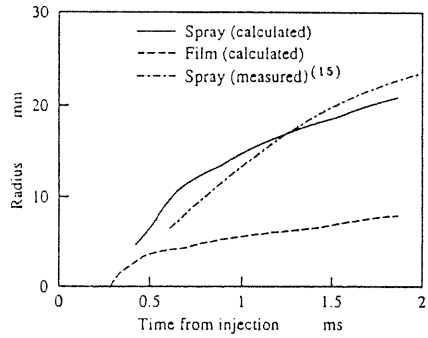

(a) Case W1

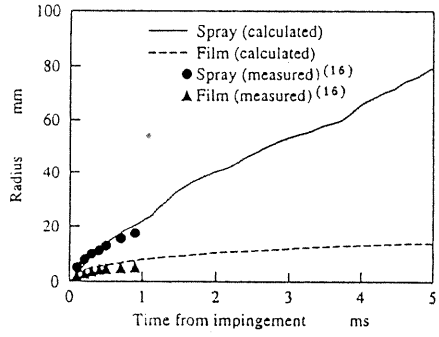

(b) Case W2

Fig. 16 Spreading radii of sprays and liquid film after impingement ($\alpha_w = 0$ deg.)

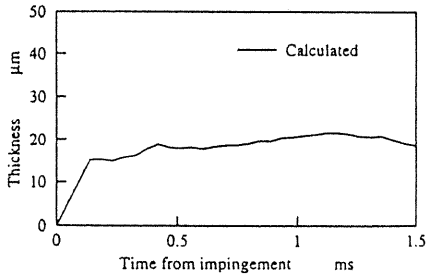

(a) Case W1

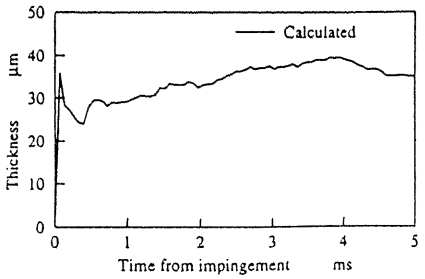

(b) Case W2

Fig. 17 Averaged thickness of liquid film ($\alpha_w = 0$ deg.)

The calculated and measured[15],[16] adherent fuel mass ratios at α_w = 0, 15 and 30 deg. for Case W1 and Case W2 are shown in Fig.15. It is found that the calculated results for both cases agree quite well with the measured data.

The spreading radii of the calculated sprays and liquid film after impingement at α_w = 0 deg. are shown in Fig.16 along with the measured data[15],[16]. The calculated results of the spray radii for Case W1 and Case W2 agree well with the experimental results. When comparing the calculated and measured radii of liquid film for Case W2, the tendency in the temporal variation of liquid film radius is well reproduced, although the calculated radius is a little larger than the measured one.

The temporal variation in the averaged thickness of the calculated liquid film at α_w = 0 deg. is shown in Fig.17. This averaged thickness is determined by dividing the mass of liquid film by the density and spreading area of the film. According to the experimental results, the averaged thickness of the liquid film for Case W1 is about 30 μm[17] and that for Case W2 is about 55 μm[16]. The levels of the calculated thickness shown in Fig.17 for both cases are lower than their respective measured values. However, the differences between the calculated and measured values are not so large.

From the above, it is shown that the present spray model can predict reasonably well the behavior of sprays impinging on a wall and the liquid film formation.

SIMULATION OF SPRAYS IN A PORT-INJECTION GASOLINE ENGINE

Using the present spray model, the behavior of sprays injected into the intake port of a gasoline engine is numerically simulated. The model engine[3] (Fig.18) is a two-intake valve engine (bore=78 mm, stroke=69.7 mm) with two directed ports which generate a tumbling vortex. During intake stroke (Θ = 0 - 180 deg.ATDC) at an engine speed of 2000 rpm, the gas flow is calculated with a crank angle interval of 1.0 deg. or 2.5 deg. in main cycles, and the spray, liquid film and fuel vapor are calculated in subcycles. The Hybrid scheme is used as the differencing scheme for convection terms to ensure the stability. As initial conditions, the temperature and pressure of air in the cylinder are set at room temperature and atmospheric pressure. The temperature of all walls is set at room temperature during intake stroke. The fuel (octane) is injected into one of the two intake ports in the form of a hollow-cone spray with the outer and inner cone angles being 20 and 10 deg., respectively. The pressure difference for injection is 300 kPa and the injection velocity is 22.7 m/s. The fuel injection starts at 20 deg.ATDC and ends at 90 deg.ATDC in intake stroke with a constant injection rate (the total number of injected droplet parcels is 2000). The total mass of injected fuel is such a quantity that the air-to-fuel ratio A/F in the cylinder becomes 22 if the liquid fuel completely vaporizes. For coping with defect of the present drop breakup model at low-pressure ambient gas, the initial diameters of droplets at the nozzle outlet are distributed using random numbers so that the initial Sauter mean radius becomes a typical value (32 μm).

Figure 19 shows the temporal variation in the distri-

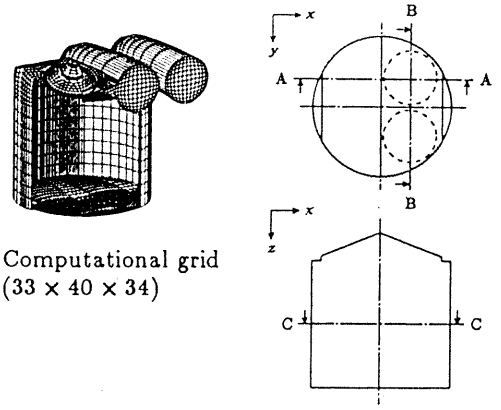

(a) Computational grid (33 x 40 x 34)

(b) Sections for plotting

Fig. 18 Model engine

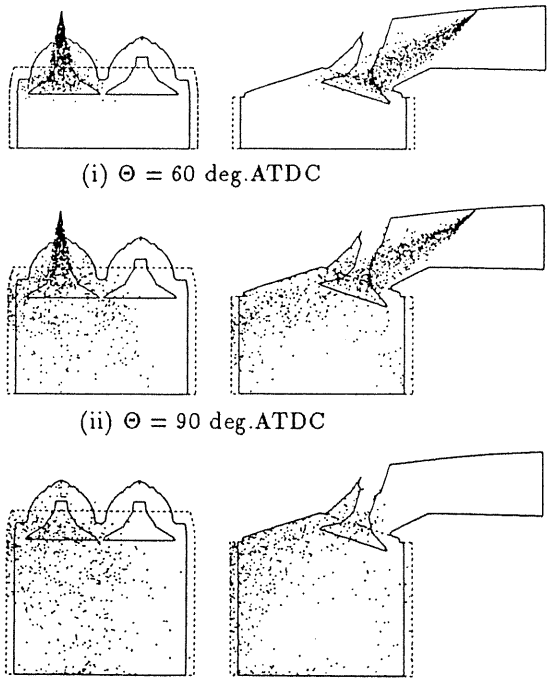

(i) Θ = 60 deg.ATDC

(ii) Θ = 90 deg.ATDC

(iii) Θ = 120 deg.ATDC

(a) Section B-B (b) Section A-A

Fig. 19 Temporal variation in droplet distribution (projections of all droplet parcels)

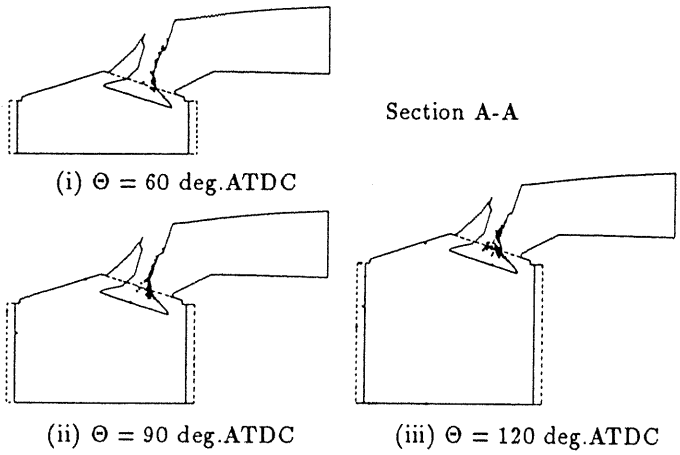

Section A-A

(i) Θ = 60 deg.ATDC

(ii) Θ = 90 deg.ATDC (iii) Θ = 120 deg.ATDC

Fig. 20 Temporal variation in liquid film distribution (projections of all liquid film parcels)

bution of droplets (projections of all droplet parcels). It is found that the spray is curved due to the intake flow, and the droplets impinge on the intake valve. As shown in Fig.20, patches of liquid film are mainly formed on the stem and neck of the valve. The distribution of fuel vapor concentration (A/F) at BDC of intake stroke is shown in Fig.21. The vapor concentration distribution in the cylinder is extremely inhomogeneous and the mixture is distributed locally under the intake port into which the fuel is injected. Figure 22 shows the temporal variation in the mass fractions of total fuel (droplets + liquid film + vapor), liquid phase (droplets + liquid film) and liquid film in the whole region. It is found that the fraction of liquid film reaches about 46 % at about 120 deg.ATDC. At BDC, about the 19 % and 34 % of the total injected fuel mass remain as liquid film and liquid phase, respectively. The amount of vapor scarcely increases until 90 deg.ATDC. It follows that the mixture formation is considerably delayed in this cold wall case.

CONCLUSIONS

A new model for fuel sprays impinging on a wall with liquid film formation is proposed in this study. This model is incorporated into the GTT code, which employs the Discrete Droplet Model along with the drop breakup model by Reitz et al. The present spray model has been tested for sprays injected in quiescent and swirling gases and for sprays impinging on a flat wall.

By comparing the calculated results with the experimental data, it has been found that the model can predict reasonably well both the spray tip penetration in high-pressure, room- or high-temperature quiescent gas and the penetration in swirling gas. For correctly predicting the droplet radius distribution in low-pressure ambient gas and also the dispersion of droplets in intense swirl, however, the drop breakup model has to be improved.

With respect to sprays impinging on a wall, the present spray model gives good predictions for the behavior of droplets and liquid film and also for the adherent fuel mass ratio. Using the present spray model, the fuel sprays injected into an intake port of a gasoline engine have been numerically simulated. The behavior of droplets and that of liquid film during intake stroke have been analyzed. It has been found that mixture formation in the cylinder is considerably delayed in the case of the cold wall.

ACKNOWLEDGMENT

This work has been partially supported by a Grant-in-Aid for Scientific Research (B(2), No.05555066) from the Ministry of Education, Science and Culture of Japan.

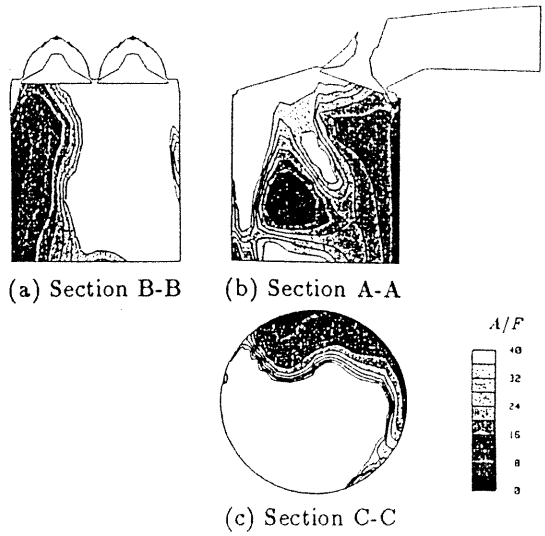

Fig. 21 Fuel vapor distribution at BDC of intake stroke

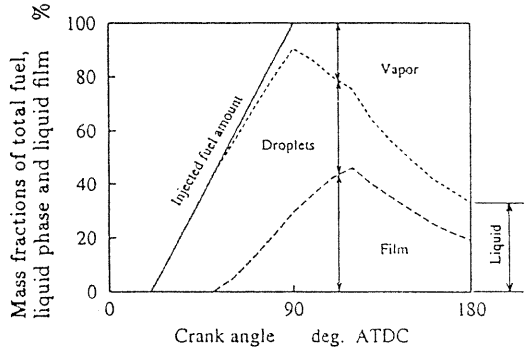

Fig. 22 Temporal variation in the mass fractions of total fuel, liquid phase and liquid film

REFERENCES

1. Amsden, A. A., et al., "KIVA", Los Alamos National Laboratory Report, LA-10245-MS, 1985.
2. Wakisaka, T., et al., Proc. 11th Symp. on Internal Combustion Engines, JSME/JSAE, pp.241-246, 1993 (in Japanese).
3. Wakisaka, T., et al., COMODIA90, JSME, pp.487-492, 1990.
4. Reitz, R. D., et al., SAE Paper 870598, 1987.
5. Yabe, T., et al., Journal of the Physical Society of Japan, Vol.57, No.8, pp.2598-2601, 1988.
6. Hiroyasu, H., et al., SAE Paper 740715, 1974.
7. Kuo, T. W., et al., SAE Paper 820133, 1982.
8. Yokota, H., et al., Trans. JSME, Ser.B, Vol.54, No.499, pp.741-748, 1988 (in Japanese).
9. Fang, C. Y., et al., Trans. JSME, Ser.B, Vol.56, No.528, pp.2510-2518, 1990 (in Japanese).
10. Hiroyasu, H., et al., Trans. JSAE, No.21, pp.339-345, 1980 (in Japanese).
11. Jayaratne, O. W., et al., Proc. Roy. Soc. London A, Vol.280, pp.545-565, 1964.
12. Toda, S., Trans. JSME, Vol.39, No.323, pp.2160-2171, 1973 (in Japanese).
13. Naber, J. D., et al., SAE Paper 880107, 1988.
14. Wachters, L. H. J., et al., Chemical Engineering Science, Vol.21, pp.1047-1056, 1966.
15. Saito, M., et al., Trans. JSME, Ser.B, Vol.57, No.543, pp.3973-3980, 1991 (in Japanese).
16. Saito, A., et al., Proc. 10th Joint Symp. on Internal Combustion Engines, JSAE/JSME, pp.361-366, 1992 (in Japanese).
17. Fujimoto, H., et al., Proc. 1st Symp. on Atomization, ILASS-Japan, pp.149-154, 1992 (in Japanese).